

Mon. Not. R. Astron. Soc. **364,** 443–454 (2005) doi:10.1111/j.1365-2966.2005.09434.x

# *Spitzer* imaging of *i′*-drop galaxies: old stars at $z \approx 6$

Laurence P. Eyles,[1⋆] Andrew J. Bunker,[1] Elizabeth R. Stanway,[2] Mark Lacy,[3] Richard S. Ellis[4] and Michelle Doherty[5]

[1]*School of Physics, University of Exeter, Stocker Road, Exeter, EX4 4QL*
[2]*Astronomy Department, University of Wisconsin-Madison, 475 N. Charter Street, Madison, WI 53706, USA*
[3]*Spitzer Science Center, California Institute of Technology, Mail Code 220-6, 1200 E. California Blvd., Pasadena, CA 91125, USA*
[4]*California Institute of Technology, Mail Stop 169-327, Pasadena, CA 91109, USA*
[5]*Institute of Astronomy, Madingley Road, Cambridge, CB3 0HA*

Accepted 2005 July 14. Received 2005 July 13; in original form 2005 February 18

**ABSTRACT**

We present new evidence for mature stellar populations with ages >100 Myr in massive galaxies ($M_{\rm stellar} > 10^{10}\,{\rm M}_{\odot}$) seen at a time when the Universe was less than 1 Gyr old. We analyse the prominent detections of two $z \approx 6$ star-forming galaxies (SBM03#1 and #3) made at wavelengths corresponding to the rest-frame optical using the Infrared Array Camera camera onboard the *Spitzer Space Telescope*. We had previously identified these galaxies in *Hubble Space Telescope (HST)* Advanced Camera for Surveys (ACS) / Great Observatories Origins Deep Survey (GOODS) images of *Chandra* Deep Field South through the '*i*′-drop' Lyman-break technique, and subsequently confirmed the identification spectroscopically with the Keck telescope. The new *Spitzer* photometry reveals significant Balmer/4000-Å discontinuities, indicative of dominant stellar populations with ages >100 Myr. Fitting a range of population synthesis models (for normal initial mass functions) to the *HST/Spitzer* photometry yields ages of 250–650 Myr and implied formation redshifts $z_{\rm f} \approx 7.5$–13.5 in presently-accepted world models. Remarkably, our sources have best-fitting stellar masses of 1.3–3.8 $\times\ 10^{10}\,{\rm M}_{\odot}$ (95 per cent confidence) assuming a Salpeter IMF. This indicates that at least some galaxies with stellar masses >20 per cent of those of a present-day $L^{*}$ galaxy had already assembled within the first Gyr after the Big Bang. We also deduce that the past average star formation rate must be comparable to the current observed rate ($\rm SFR_{UV} \sim 5$–$30\,{\rm M}_{\odot}\,{\rm yr}^{-1}$), suggesting that there may have been more vigorous episodes of star formation in such systems at higher redshifts. Although a small sample, limited primarily by *Spitzer's* detection efficiency, our result lends support to the hypothesis advocated in our earlier analyses of the Ultra Deep Field and GOODS *HST*/ACS data. The presence of established systems at $z \approx 6$ suggests that long-lived sources at earlier epochs ($z > 7$) played a key role in reionizing the Universe.

**Key words:** galaxies: high redshift – galaxies: individual: SBM03#1 – galaxies: individual: SBM03#3 – galaxies: individual: GLARE#3001 – galaxies: individual: GLARE#3011 – galaxies: stellar content.

## 1 INTRODUCTION

In recent years, advances in detector efficiency, large ground-based telescopes and space-based observatories such as the *Hubble Space Telescope (HST)* and *Spitzer Space Telescope*, have revolutionized studies of the high redshift Universe. Searches based on Lyman $\alpha$ (Ly$\alpha$) emission are now at last uncovering many galaxies at $2 < z < 7$ (e.g. Kodaira et al. 2003; Rhoads et al. 2004). The Lyman-break technique (Steidel, Pettini & Hamilton 1995; Steidel et al. 1996, 1999) has likewise proved successful in selecting high-redshift star-forming galaxies. This utilizes the rest-UV continuum break seen shortwards of Ly$\alpha$ and caused by H I absorption in the intergalactic medium. The redshift range $z \approx 6$ is of great importance, as it heralds the end of the reionization of the Universe (Becker et al. 2001; Kogut et al. 2003) which might be achieved through star formation. Using *HST* and the new Advanced Camera for Surveys (ACS; Ford et al. 2003), the Lyman-break technique has been pushed to this early epoch (Stanway, Bunker & McMahon 2003; Bouwens et al. 2004a; Yan & Windhorst 2004;

⋆E-mail: eyles@astro.ex.ac.uk

Giavalisco et al. 2004) by using the $i'$ and $z'$ filters to isolate $i'$-drop galaxies. Ground-based follow-up spectroscopy (Bunker et al. 2003; Stanway et al. 2004a,b; Dickinson et al. 2004) has shown that a colour cut of $(i' - z')_{AB} > 1.5$ mag reliably finds star-forming galaxies at $z \approx 6$ with modest foreground contamination (primarily from low-mass stars, and passively evolving galaxies at $z \sim 1 - 2$). Subsequent low-dispersion slitless spectroscopy with *HST*/ACS (Malhotra et al. 2005) confirms the nature of $i'$-drops as $z \sim 6$ galaxies with a small contaminant fraction of stars and low-redshift sources.

Yet an important part of the puzzle is missing: the $i'$-band drops are selected in the rest-frame UV, and are therefore known to be actively forming stars. However, it is unclear whether these objects suffer from significant reddening due to dust (in which case the star formation rates will have been underestimated), or if there is an underlying older stellar population which has been recently rejuvenated. Publicly available *Spitzer* imaging with the Infrared Array Camera (IRAC; Fazio et al. 2004) as part of the Great Observatories Origins Deep Survey[1] (GOODS; Dickinson & Giavalisco 2003; Dickinson et al., in preparation) allows us to address both questions.

A key benefit of *Spitzer* photometry arises because the IRAC camera samples wavelengths longwards of the age-sensitive Balmer and 4000-Å breaks at $z \approx 6$. Accordingly, we have analysed the IRAC images of the GOODS-South field (centred on the *Chandra* Deep Field South, Giacconi et al. 2002), where we have already selected $i'$-drop galaxies from the GOODS-South ACS images (Stanway et al. 2003) and the Ultra-Deep Field (UDF; Bunker et al. 2004).

Our goal in this paper is thus to focus on the infrared properties of four $z \approx 6$ galaxies for which there are robust spectroscopic redshifts, based on Ly$\alpha$ emission. The properties of the entire $i'$-drop population in the GOODS fields is considered in a forthcoming paper (Eyles et al., in preparation). Our four confirmed sources include two sources from Stanway et al. (2003): the brightest confirmed $i'$-drop in the GOODS-South field (with $z' = 24.7$ mag) SBM03#3 [with a spectroscopic redshift of $z = 5.78$ from the Deep Imaging Multi-Object Spectrograph (DEIMOS) on Keck II, Bunker et al. 2003]; and the brightest $i'$-drop in the UDF, SBM03#1 with $z' = 25.3$ mag (spectroscopically confirmed with Keck/DEIMOS by Stanway et al. 2004a as having a redshift of $z = 5.83$). Both of these spectroscopic redshifts were independently confirmed by Dickinson et al. (2004). The other two sources come from the Gemini Ly$\alpha$ at Reionization Era (GLARE, Stanway et al. 2004b) spectroscopy with the Gemini Multi-Object Spectrograph (GMOS): GLARE#3001 ($z = 5.79$, $z' = 26.4$ mag) and GLARE#3011 ($z = 5.94$, $z' = 27.2$ mag).

A plan of the paper follows. In Section 2 we describe the *Spitzer* imaging data and the methods used to fit stellar populations to the broad-band photometry derived collectively from *Spitzer*, *HST* ACS and Near Infrared Camera and Multi-Object Spectrometer (NICMOS) images, as well as ground-based near-infrared data. We discuss the implications of the age and stellar mass estimates in Section 3. Our conclusions are presented in Section 4. Throughout we adopt the standard 'concordance' cosmology[2] of $\Omega_M = 0.3$, $\Omega_\Lambda = 0.7$, and use $H_0 = 70\,\mathrm{km\,s^{-1}\,Mpc^{-1}}$. In this cosmology, the Universe today is 13.67 Gyr old, and at $z = 5.8$ the age was 992 Myr. All magnitudes are based on the *AB* system (Oke & Gunn 1983).

## 2 OBSERVATIONS, DATA REDUCTION AND STELLAR POPULATION FITTING

### 2.1 *Spitzer* observations

We concentrate here on the shortest-wavelength *Spitzer* images of GOODS-South taken with IRAC as part of the 'Super Deep' Legacy programme (Proposal ID 194, Dickinson et al., in preparation). We have analysed the first half of the GOODS-South *Spitzer* data, taken with 39 astronomical observation requests (AORs) observed between 2004 February 8–16.

The IRAC comprises four channels, each with a $256^2$ InSb array imaging a $5.2 \times 5.2$ arcmin$^2$ field with a pixel size of $\approx$1.22 arcsec. Images were taken through four broad-band infrared filters, with central wavelengths at approximately $\lambda_{\mathrm{cent}} = 3.6$, 4.5, 5.6 and 8.0 μm (channels 1–4), and widths of $\Delta\lambda_{\mathrm{FWHM}} = 0.68$, 0.87, 1.25 and 2.53 μm respectively (Fig. 1). The individual frame times for each channel were 200 s (except those taken at 8.0 μm, which comprise four integrations of 50 s at each position). Over the course of the 39 AORs, a large $2 \times 2$ mosaic of pointings was executed, with smaller random sub-dithers when the pattern was repeated, giving a $10 \times 10$ arcmin$^2$ coverage for each filter. Each AOR consisted of 10–11 pointings. Channels 1 and 3 (3.6 and 5.6 μm) have the same pointing, offset by 6.7 arcmin from the common pointing of channels 2 and 4 (4.5 and 8.0 μm). As a result, only a portion of the field is observed in all four wavebands. Once data from the second epoch (when the telescope has rotated by 180 degrees) have been gathered, images of the entire $10 \times 16.5$ arcmin$^2$ field matching the GOODS-South ACS survey (Giavalisco 2003) in all four filters will be available. Meanwhile, by design, the overlap region common to all filters covers the Ultra Deep Field (Beckwith, Somerville & Stiavelli 2003). The total exposure time in each channel is $\approx$ 86 ks, depending on location.

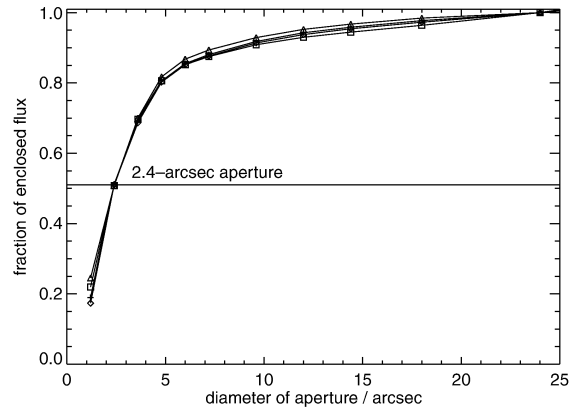


**Figure 1.** The fractional flux enclosed within a circular aperture as a function of aperture diameter, determined from four bright but unsaturated isolated point sources in the IRAC channel 1 (3.6 μm) GOODS-South image. The small aperture used for faint sources (2.4-arcsec diameter) is marked: this encircles 52 per cent of the energy, implying an aperture correction of 0.7 mag. Note that the official *Spitzer* calibration for IRAC uses a 24-arcsec-diameter aperture, so the fraction of the flux there is set to 1.0 by definition.

[1] see http://www.stsci.edu/ftp/science/goods/

[2] Adopting the first-year *WMAP* best-fitting cosmology from Spergel et al. (2003) with $\Omega_M = 0.27$, $\Omega_\Lambda = 0.73$, and $H_0 = 71\,\mathrm{km\,s^{-1}\,Mpc^{-1}}$ makes a negligible difference: the masses and luminosities would be 4 per cent greater, and the Universe would be 4 per cent younger at $z = 5.8$.

**Table 1.** The four spectroscopically-confirmed $i'$-drop galaxies in the GOODS-South Field.

| ID | RA (J2000) | Dec. (J2000) | Redshift | Age of Universe/Gyr |
|---|---|---|---|---|
| SBM03#1[a] | 03:32:40.01 | −27:48:15.0 | 5.83 | 0.95 |
| SBM03#3 | 03:32:25.61 | −27:55:48.7 | 5.78 | 0.96 |
| GLARE#3001 | 03:32:46.04 | −27:49:29.7 | 5.79 | 0.96 |
| GLARE#3011 | 03:32:43.10 | −27:45:17.6 | 5.94 | 0.93 |

[a]This is also known as GLARE#1042 (Stanway et al. 2004b), #20104 (Bunker et al. 2004), SiD002 (Dickinson et al. 2004) and YW01a (Yan & Windhorst 2004).

### 2.2 Data reduction

For our investigation, we used the pipeline-processed IRAC images at the 'post-basic calibrated data' (PBCD) stage,[3] details of which can be found in the Infrared Array Camera Data Handbook, Version 1.0 (Reach et al. 2004). The main steps in the pipeline include dark current subtraction, application of flat fields, flux calibration (in units of MJy sr$^{-1}$) and mosaicking of the individual frames of each AOR after application of a distortion correction. PBCD sets have a refined pointing solution to an accuracy of 0.2 arcsec derived from the Two-Micron All Sky Survey point source catalogue objects in the field of view. Outlier rejection is performed during the mosaicking process.

We used the Image Reduction and Analysis Facility IRAF to combine the 39 PBCD mosaics (one for each AOR), which were taken at different telescope roll angles. The IRAF task WREGISTER was used to rotate the frames to a common roll angle. The individual registered frames were scaled to the same integration time and all the frames were offset by the median counts in the centre of the area (which was common to all frames) to account for floating bias levels; the 39 frames were combined using IMCOMBINE (weighting by the exposure times). During this, residual unrejected cosmic rays, bad pixels, and the column pull-down and MUXBLEED detector effects were removed using a percentile clipping method 'pclip', rejecting at the $3\sigma$ level. The PBCD images were converted from units of surface brightness (MJy sr$^{-1}$) into flux units of μJy per pixel by multiplying the data units by $10^{12}$ × (pixel solid angle): a numerical factor of 34.98. The images were matched to the v1.0 reduced $z'$-band tiles of the GOODS-South field released by the GOODS team.[4] The astrometry was found to be consistent to within ≈0.2 arcsec. While our reduction was underway, the GOODS team released an enhanced data set (DR1),[5] employing a 'multidrizzle' technique similar to that used successfully on *HST*/ACS GOODS data. This provides combined images with a pixel scale of ≈0.6 arcsec. The magnitudes listed in this paper are determined from this 'drizzled' data, and we have used our independent reduction as a consistency check. Upon cross-checking the astrometry, photometry and noise properties, they were found to be consistent to 0.1 mag (for bright sources) and 0.2 arcsec.

In the final GOODS-South co-added DR1 'drizzled' images, we measured the full width at half-maximum (FWHM) of the point spread function (PSF) to be ≈1.5 arcsec in channels 1 and 2 (3.6 and 4.5 μm), ≈1.8 arcsec in channel 3 (5.6 μm) and ≈2.1 arcsec in channel 4 (8 μm). Even for the short-wavelength IRAC images, the *Spitzer* PSF is much larger than the typical size of the $z \approx 6$ $i'$-band drop galaxies (whose half-light radii $r_{\rm hl} < 0.2$ arcsec, Bunker et al. 2004). At *Spitzer* resolution, these galaxies are clearly unresolved and so we treat them as point sources.

To construct spectral energy distributions of our four spectroscopically confirmed $i'$-band drop galaxies in the GOODS-South field (detailed in Section 1 and Table 1) we undertook aperture photometry in the various images. In order to maximize the signal-to-noise ratio (S/N) and to minimize possible confusion with other foreground objects, we used a diameter ≈1.5 × FWHM for the IRAC images, appropriate for unresolved objects. The aperture diameters were 4, 4, 5 and 6 'drizzled' pixels for the 4 channels (3.6, 4.5, 5.6 and 8.0 μm), corresponding to 2.4, 2.4, 3.0 and 3.7 arcsec, respectively. We used the IRAF `digiphot.phot` package to measure the enclosed flux at the exact coordinates determined from the GOODS v1.0 and UDF $z'$-band images, taking the residual background from an annulus between 12 and 24 arcsec radius. We applied aperture corrections to compensate for the flux falling outside the aperture: these were ≈0.7 mag, as determined from bright but unsaturated point sources in the images, with apertures of diameter 18 arcsec in channels 1 and 2, 24 arcsec in channel 3 and 30 arcsec in channel 4. The curve of growth for four stars is shown in Fig. 1 (note that the official *Spitzer* calibration for IRAC also uses a similar 24-arcsec-diameter aperture, so the aperture correction there is 1.0 by definition). These aperture corrections are consistent with those derived for the First Look Survey (Lacy et al. 2005).

The galaxy images in the various wavebands are shown in Figs 2, 3, 4 and 5. Checks were made to ensure that the objects were not contaminated by the presence of any neighbouring bright foreground sources. An object was deemed to be uncontaminated if no bright source lay within a 4-arcsec radius from it. All four objects satisfied this criterion; the bright source close to SBM03#3 lies on the 4-arcsec limit (Fig. 3). The *Spitzer* magnitudes in Table 2 have the neighbour subtracted out (i.e. are deblended) but this has only ≈5 per cent effect on the measured flux in our 2.4-arcsec-diameter aperture; less than the error bar. The subtraction of the neighbour was done using the GALFIT software (Peng et al. 2002). This takes into account the PSF (we give it a PSF for the drizzled image derived from stacking four bright but isolated stars) and a best-fitting galaxy surface brightness profile. An exponential disc worked best in the case of this neighbour, but it is not very sensitive to the exact functional form with the poor resolution of *Spitzer*. Fig. 4 shows the postage-stamp image of SBM03#3 with the model fit of the neighbour subtracted.

The noise for each of the four channels was checked in two different ways. First, we derived an estimate based on a Poisson model using the detector gain, number of frames combined, and the background counts (adding back the zodiacal background estimate subtracted by the pipeline but recorded in the header). Secondly, we measured the standard deviation in background counts of the images. As the mosaicking process introduces correlations between pixels, we also made noise estimates using the individual BCDs and

[3] The PBCD images are available from http://data.spitzer.caltech.edu/popular/goods/irac_04/

[4] Available from ftp://archive.stsci.edu/pub/hlsp/goods/v1

[5] For the enhanced data set GOODS DR1 see http://data.spitzer.caltech.edu/popular/goods/Documents/goods_dr1.html.

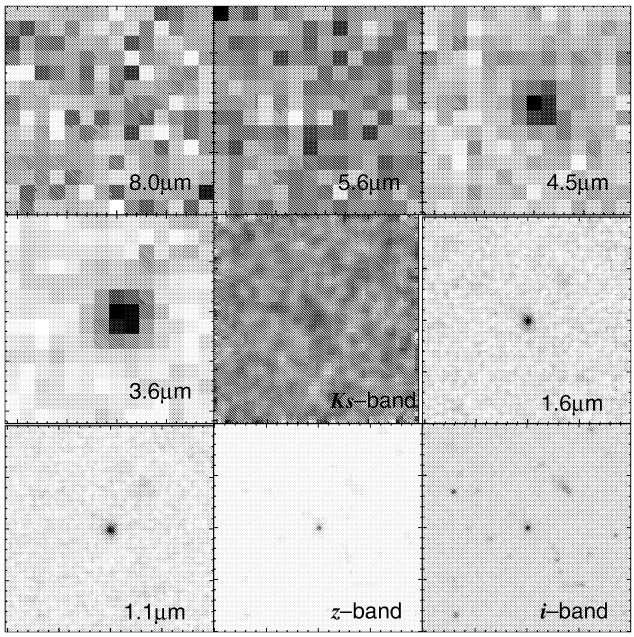


**Figure 2.** Images of SBM03#1 ($z = 5.83$), taken with *HST*/ACS ($i'$- and $z'$-band); *HST*/NICMOS (1.1 μm F110W '$J$-band', and 1.6 μm F160W '$H$-band'), VLT/ISAAC $K_s$-band (smoothed with a 3-pixel 0.45-arcsec boxcar) and the four *Spitzer* channels (3.6–8.0 μm). Each panel is 8 arcsec across (a projected distance of 50 kpc).

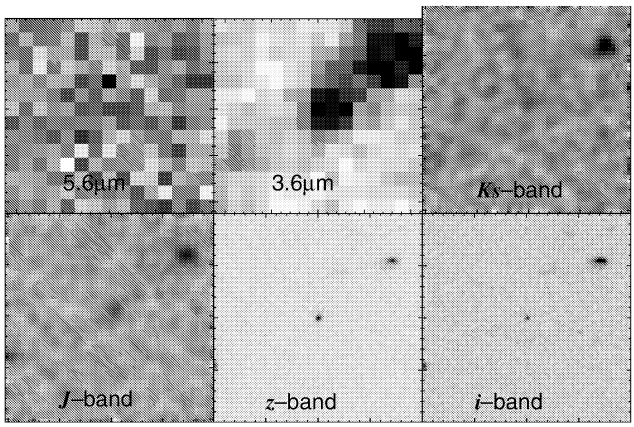


**Figure 3.** Images of SBM03#3 ($z = 5.78$), taken with *HST*/ACS ($i'$- and $z'$-band); VLT/ISAAC $J$- and $K_s$-bands and *Spitzer* channels 3.6 and 5.6 μm. Each panel is 8 arcsec across (a projected distance of 50 kpc). The $J$ and $K_s$ band images have been smoothed using a 3-pixel box.

assuming it decreased as the square root of the number of frames. These estimates lead to $3\sigma$ limiting AB magnitudes of 26.5 and 26.1 in 2.4-arcsec apertures in channels 1 and 2, respectively, and 23.8 and 23.5 in 3.0 arcsec apertures in channels 3 and 4, respectively. There will be additional background fluctuations caused by faint galaxies (i.e. confusion noise), which will increase the noise. Both methods produce consistent estimates.

Table 2 lists the measured AB magnitudes (corrected to approximate total magnitudes through an aperture correction) for the IRAC 3.6, 4.5 and 5.6 μm channels. None of the sources

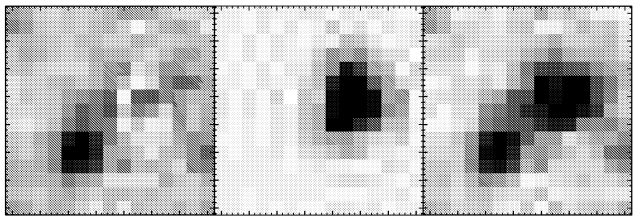

**Figure 4.** *Spitzer* channel 1 (3.6 μm) image of SBM03#3 (right, lower-left of panel), with the best-fitting GALFIT model for the surface brightness profile of the nearby neighbour (middle image, an exponential disc convolved with the PSF), and the *Spitzer* image with the neighbouring galaxy subtracted (left). The photometry of SBM03#3 is only affected at the ∼5 per cent level by confusion from the neighbour. The frame is 9 arcsec across.

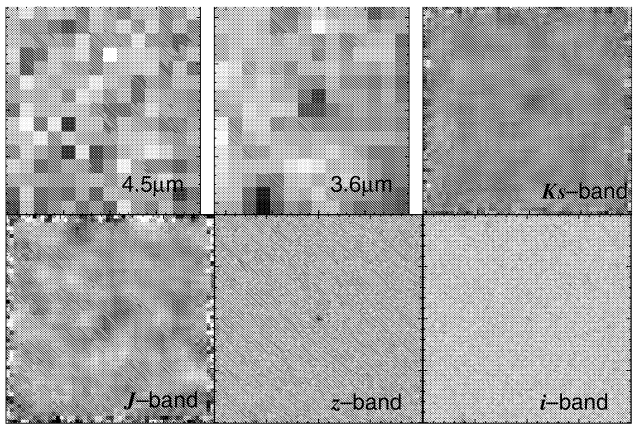


**Figure 5.** Images of GLARE#3001 ($z = 5.79$), taken with *HST*/ACS ($i'$- and $z'$-band); VLT/ISAAC $J$- and $K_s$-bands and *Spitzer* channels 3.6 and 4.5 μm. Each panel is 8 arcsec across (a projected distance of 50 kpc). The $J$ and $K_s$ band images have been smoothed using a 5-pixel box.

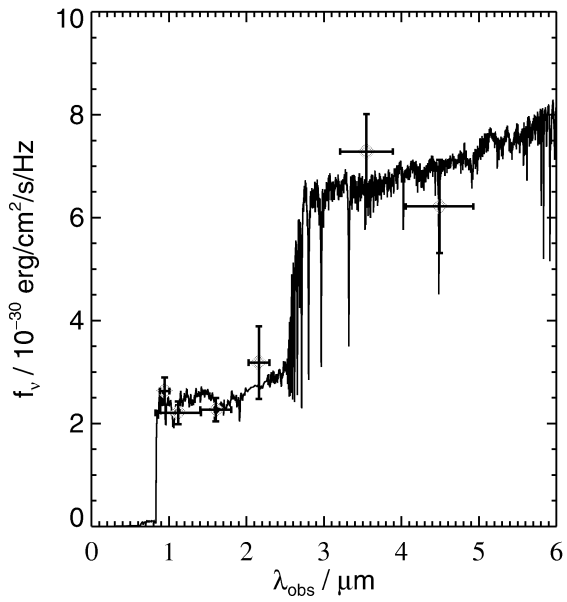


**Figure 6.** Best-fitting Bruzual & Charlot model for SBM03#1: an exponentially decaying star formation rate with $\tau = 300$ Myr, viewed 640 Myr after the onset of star formation. The stellar mass is $3.4 \times 10^{10}\,M_\odot$. Flux density is in $f_\nu$ units.

**Table 2.** Magnitudes (AB system) of four $i'$-band drop galaxies. SBM03#3 is not in the field of view for the 4.5 μm and 8.0 μm filters. The galaxies are undetected at 8.0 μm, with AB > 23.5 ($3\sigma$).

| ID | $i'$ | $z'$ | $J$ | $K_s$ | 3.6 μm | 4.5 μm | 5.6 μm |
|---|---|---|---|---|---|---|---|
| SBM03#1 | $26.99 \pm 0.03$ | $25.35 \pm 0.02$ | $25.54^a \pm 0.04$ | $25.14 \pm 0.22$ | $24.24 \pm 0.09$ | $24.42 \pm 0.15$ | >23.8 ($3\sigma$) |
| SBM03#3 | $26.27 \pm 0.13$ | $24.67 \pm 0.03$ | $24.72 \pm 0.15$ | $25.55 \pm 0.40^b$ | $23.94 \pm 0.07$ | – | $24.39 \pm 0.69$ |
| GLARE#3001 | $28.03 \pm 0.14$ | $26.37 \pm 0.06$ | $26.11 \pm 0.32$ | $25.22 \pm 0.32$ | $25.88 \pm 0.36$ | >26.1 ($3\sigma$) | >23.8 ($3\sigma$) |
| GLARE#3011 | >28.8 ($3\sigma$) | $27.15 \pm 0.12$ | >26.2 ($3\sigma$) | >25.6 ($3\sigma$) | >26.5 ($3\sigma$) | >26.1 ($3\sigma$) | >23.8 ($3\sigma$) |

[a] From NICMOS F110W imaging (Stanway, McMahon &Bunker 2005), rather than ESO VLT/ISAAC imaging. The NICMOS F160W magnitude of SBM03#1 is $H_{AB} = 25.51 \pm 0.05$. [b] The $K_s$ magnitude of SBM03#3 is anomalously faint.

was detected at $>3\sigma$ in the 5.6 or 8 μm channels, although SBM03#3 has a very marginal ($2\sigma$) detection at 5.6 μm ($AB = 24.4 \pm 0.7$). In the short-wavelength channels, SBM03#1 & #3 are well-detected ($>10\sigma$, $AB \approx 24$), and we have a more marginal $3\sigma$ detection of GLARE#3001 ($z'_{AB} = 26.4$) at $AB \approx 26$. Only SBM03#1 is detected at 4.5 μm – SBM03#3 falls outside the region surveyed so far in this filter, and GLARE#3001 is undetected. The fainter GLARE#3011 ($z'_{AB} = 27.2$) was undetected at all IRAC wavelengths. For the *HST* photometry, we use the ACS $i'$-band and $z'$-band magnitudes from Stanway et al. (2003) from GOODS-South and, in the case of SBM03#1, from the deeper UDF (Bunker et al. 2004). These magnitudes are already corrected to a total flux, also through an aperture correction. We use NICMOS magnitudes (Thompson et al. 2005) in F110W and F160W ($J$ and $H$ bands) from Stanway, McMahon & Bunker (2005) for SBM03#1, and for the others we used v1.0 of the European Southern Observatory (ESO) Very Large Telescope (VLT)/Infrared Spectrometer and Array Camera (ISAAC) GOODS/ESO Imaging Survey (EIS) images [6] in the $J$ and $K_s$ bands (Vandame et al., in preparation). In the ground-based near-infrared ISAAC images, we used 1-arcsec-diameter apertures. The seeing varied across the ISAAC field, as different tiles were taken over many nights, so we determined the aperture correction from unresolved sources in each tile. For the $J$- and $K_s$-band images the seeing is typically good (FWHM $= 0.4 - 0.5$ arcsec), and the aperture correction is ≈0.3–0.5 mag, determined from bright but unsaturated isolated stars measured in 6-arcsec-diameter apertures.

The galaxy SBM03#3 is towards the edge of the released ESO/VLT imaging, where fewer frames overlap and the noise is higher. Its $K_s$ magnitude seems to be anomalously faint (a $3\sigma$ detection at $K_{AB} = 25.5$, twice as faint as the shorter-wavelength $z'$ and $J$, which have $AB = 24.7$ mag, and four times fainter than the longer-wavelength IRAC 3.6-μm detection at $AB = 24.0$). We still include the $K_s$ filter in the fitting of the stellar populations (Section 2.3), but caution that the $K_s$ magnitude may not be reliable. Fortunately, this filter makes minimal difference to the best-fitting populations as its statistical weighting is low.

### 2.3 Spectral energy distributions

The final step in the reduction process is the construction of spectral energy distributions (SEDs) for the chosen sources. Spitzer photometry and SED fitting has already produced great insight into the $z = 2 - 3$ Lyman-break star-forming galaxies (Barmby et al. 2004; Shapley et al. 2005) and here we apply similar techniques at $z \approx 6$. In order to compare our photometry with stellar spectral synthesis models, we utilize the latest Bruzual & Charlot (2003, hereafter B&C) isochrone synthesis code. We use the Padova evolutionary tracks (preferred by B&C). The models utilize 221 age steps from $10^5$ to $2 \times 10^{10}$ yr, approximately logarithmically spaced. Models with Salpeter (1955) initial mass functions (IMF) were selected, although in Section 3.5 we also consider the effect of adopting a Chabrier (2003) IMF. There are 6900 wavelength steps, with high resolution (FWHM 3 Å) and 1-Å pixels over the wavelength range of 3300 – 9500 Å (unevenly spaced outside this range). From the full range of metallicities offered by the code, we considered both solar and 1/5 solar models. From several star formation histories available, a single stellar population (SSP – an instantaneous burst), a constant star formation rate (SFR), and exponentially decaying ($\tau$) SFR models were used. This latest version of the B&C models includes an observationally motivated prescription for thermally pulsing asymptotic giant branch (TP-AGB) stars (Liu, Graham & Charlot 2002), and also the TP-AGB multimetallicity models of Vassiliadis & Wood (1993).

For each of the four $i'$-drops with spectroscopic redshifts, the filters were corrected to their rest frame wavelengths by the appropriate redshift factor. The measured flux was folded through the filter transmission profiles, and the best-fitting age model was computed by minimizing the reduced $\chi^2$, using the measured errors on the magnitudes. The number of degrees of freedom is the number of independent data points (magnitudes in different wavebands). The Bruzual & Charlot spectra are normalized to an initial mass of $1\,M_\odot$ for the instantaneous burst SSP model, and an SFR of $1\,M_\odot\,yr^{-1}$ for the continuous star formation model. The fitting routine returned the normalization for the model which was the best fit to the broad-band photometry (i.e. minimized the reduced $\chi^2$) – this normalization was then used to calculate the corresponding best-fitting stellar mass (see Section 3.3).

For SBM03#1, the SED-fitting process was conducted using photometry from the detections in the $z'$, F110W, F160W, $K_s$, 3.6 μm and 4.5 μm filters, whilst for SBM03#3 the $z'$, $J$, $Ks$, 3.6 μm and 5.6 μm data were used.

Although some of our data points (particularly from the *HST*/ACS imaging) have S/N > 10, we set the minimum magnitude error to be $\Delta(\text{mag}) = 0.1$ to account for flux calibration uncertainties. During the SED-fitting process, the $i'$-band flux was ignored, as this band is prone to contamination due to Ly$\alpha$ forest absorption shortwards of Ly$\alpha$ ($\lambda_{\rm rest} = 1216$ Å) and also emission-line contamination due to Ly$\alpha$ itself.

## 3 ANALYSIS

For two of the spectroscopically-confirmed galaxies (SBM03#1 and #3) we have robust *Spitzer* detections at 3.6 μm of $AB \approx 24$ mag ($>10\sigma$), with the fainter GLARE sources marginally detected (GLARE#3001) or undetected (GLARE#3011). Progressing in increasing wavelength from the *HST*/ACS $z'$-band and near-infrared

[6] Available from http://www.eso.org/science/goods/releases/20040430/

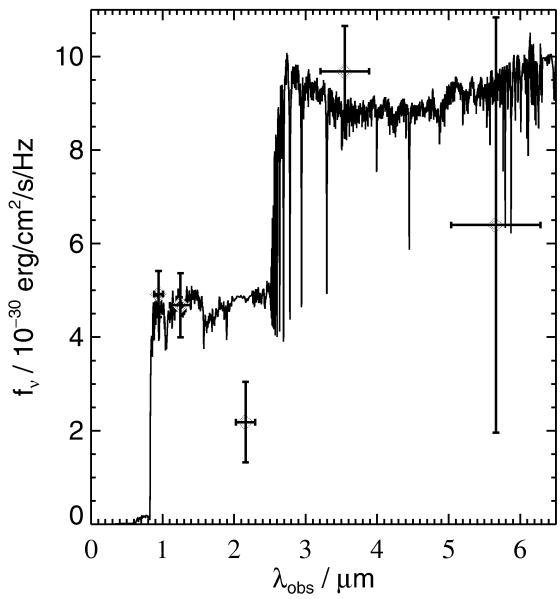


**Figure 7.** Best-fitting Bruzual & Charlot model for SBM03#3: an exponentially decaying star formation rate with $\tau = 500$ Myr, viewed 640 Myr after the onset of star formation, and with a stellar mass of $4.8 \times 10^{10}$ M$_\odot$. Flux density is in $f_\nu$ units.

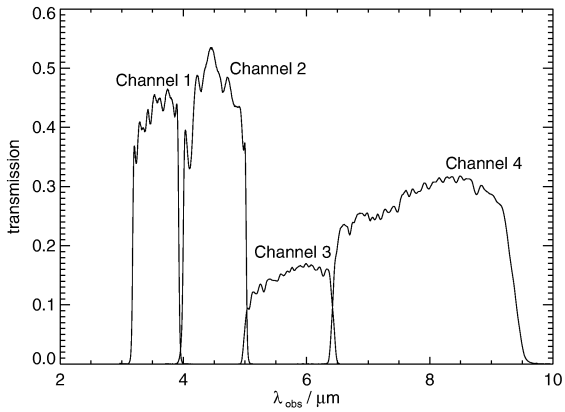


**Figure 8.** Filter profiles of the four *Spitzer* infrared wavebands.

(0.9–2.2 μm) to the *Spitzer*/IRAC 3.6 μm channel, the two well-detected $i'$-drops brighten by $\Delta(\mathrm{mag})_{AB} = 0.8$ (Figs 6 and 7) – a factor of 2 in flux density, $f_\nu$. SBM03#1 is also robustly detected with a similar magnitude at 4.5 μm. We now consider the implications of the spectral energy distributions of these $i'$-drops, specifically which star formation histories can produce the observed spectral breaks between 2.2–3.6 μm.

### 3.1 Balmer/4000-Å breaks in $z \approx 6$ galaxies

The presence of a Balmer/4000-Å break is suggestive of a system viewed a significant time after a major epoch of star formation – the Balmer break at 3648 Å is strongest in an A-star population, and metal-line blanketing (predominantly Fe II) due to an older late-type stellar population produces the 4000-Å break. For the two $i'$-drops with the best *Spitzer* detections (SBM03#1 and #3) we find evidence of a significant Balmer/4000-Å break: the brightening by a factor of 2 in $f_\nu$ from the near-infrared (≈0.9–2.2 μm) to 3.6 μm implies a break amplitude of ≈1.7 (for $f_\lambda$ flux densities). The $z'$, $J$ and $K_s$ colours are relatively flat in $f_\nu$ (Figs 6 and 7) – ignoring the discrepantly faint $K_s$ magnitude of SBM03#3– which favours the spectral break interpretation rather than dust reddening (see Section 3.5). The break amplitude of ≈1.7 is comparable to that seen by Le Borgne et al. (2005) in massive post-starburst galaxies at much lower redshifts ($z \sim 1$) from the Gemini Deep Deep Survey project. Indeed, the break amplitude in our two significant $z \approx 6$ cases is only slightly less than the $D4000$ (Bruzual 1983) observed at $z \approx 0$ in the Sloan Digital Sky Survey (e.g. Kauffmann et al. 2003), with $D4000 \approx 1.7$–2.0.

For all the galaxies discussed here, there has been recent or ongoing formation of at least *some* massive stars prior to the epoch of observation, as our Keck/Gemini spectra show Ly$\alpha$ emission produced through photoionization of hydrogen by the short-lived OB stars (Bunker et al. 2003; Stanway et al. 2004b). In order to produce the Balmer/4000-Å break amplitude at $\lambda_{\rm rest} \approx 4000$ Å, most of the stellar mass probably formed well before the current starburst, most likely >100 Myr previously (Section 3.2). Hence the galaxies SBM03#1 and #3 are already, to some extent, established systems. This is a significant finding since, at $z \approx 6$, the Universe is less than 1 Gyr old.

There is no significant evidence for a Balmer/4000-Å break in the two (fainter) spectroscopically confirmed $i'$-drops: the 3$\sigma$ detection of GLARE#3001 at 3.6 μm suggests a break of $0 \pm 0.5$ mag, and the non-detection of GLARE#3011 places a 3$\sigma$ upper limit of $\Delta AB = 1$ mag on the break amplitude. Hence the constraints for the stellar ages of GLARE#3001 and 3011 are weak, but they are consistent with younger stellar populations than SBM03#1 and #3, which are brighter and presumably more massive. In the remainder of this discussion, we focus on these two brighter sources which have significant *Spitzer* detections for which we can estimate the stellar ages and masses.

### 3.2 Ages of the $i'$-drop galaxies

We explored the best-fitting stellar ages and star formation histories of the galaxies SBM03#1 and #3 by comparing the SEDs from our broad-band photometry with the population synthesis models of B&C. We cover a range of star formation histories (presented in Tables 3–7) designed to bracket most plausible evolution scenarios. Only a subset of these star formation histories provided acceptable fits to our photometry. We now discuss several classes of model and their validity.

We begin by considering an idealized 'simple stellar population' (SSP) model, where a galaxy is viewed some time after its entire stellar mass formed in an instantaneous burst. These models provide relatively poor fits (reduced $\chi^2 \approx 3$ for solar metallicity) to our data. This is understandable given that we know that there is at least *some* ongoing star formation in both galaxies. The SSP models provide an absolute lower age limit for the bulk of the stellar mass. These SSP models yield an age of ≈100 Myr for the best-fitting population (and >70 Myr at 99 per cent confidence) in the absence of dust reddening (see Section 3.5), implying a formation redshift of $z_{\rm f} \gg 6.4$.

At the other extreme, a constant star formation history was considered. The best-fitting ages in this simplistic scenario are 1.5–5 Gyr for metallicity 0.2–1 Z$_\odot$ (with SBM03#3 best fit with a younger population than SBM03#1, and lower metallicities decreasing the age); these ages are obviously unphysical, as they exceed the age of the universe at this redshift (≈1 Gyr). This strongly implies that we are seeing both galaxies at an epoch when the star formation

**Table 3.** Favoured model parameters of various SED fits for SBM03#1, metallicity = $Z_\odot$. We varied age between 0 and 20 Gyr, and extinction between 0.00 and 1.00. We list both the mass currently in stars ($M_{\rm stellar}$), and the total baryonic mass ($M_{\rm total}$, which includes the mass returned to the IGM by evolved stars) for each star formation history.

| Model | Reduced $\chi^2_{\rm min}$ | Age (Myr) | $E(B-V)$ | $M_{\rm tot}$ ($10^{10}$ M$_\odot$) | $M_{\rm stellar}$ ($10^{10}$ M$_\odot$) | Current SFR (M$_\odot$ yr$^{-1}$) | $b$ ($10^{-10}$ yr$^{-1}$) |
|---|---|---|---|---|---|---|---|
| burst (SSP) | 2.83 | 90.5 | 0.00 | 1.35 | 1.13 | 0.00[a] | 0.00 |
| $\tau = 10$ Myr | 2.81 | 102 | 0.00 | 1.34 | 1.14 | 0.05[a] | 0.04 |
| $\tau = 30$ Myr | 2.34 | 143 | 0.02 | 1.63 | 1.36 | 4.59 | 3.38 |
| $\tau = 70$ Myr | 1.61 | 255 | 0.00 | 2.05 | 1.68 | 7.88 | 4.69 |
| $\tau = 100$ Myr | 1.38 | 321 | 0.00 | 2.33 | 1.97 | 9.80 | 4.20 |
| $\tau = 300$ Myr | 0.94 | 641 | 0.00 | 3.41 | 2.70 | 15.2 | 4.97 |
| $\tau = 500$ Myr | 0.90 | 905[b] | 0.00 | 4.35 | 3.38 | 17.0 | 5.03 |
| $\tau = 1000$ Myr | 0.97 | 1280[b] | 0.00 | 5.46 | 4.21 | 21.1 | 5.01 |
| continuous | 1.15 | 5000[b] | 0.00 | 7.93 | 5.84 | 15.9 | 2.72 |

[a]Ruled out because SFR below lower limit set by Ly$\alpha$ emission. [b]Ruled out as age is close to or exceeds 1 Gyr, age of Universe at $z \approx 6$.

**Table 4.** Favoured model parameters of various SED fits for SBM03#1, metallicity = $0.2\,Z_\odot$. We varied age between 0 and 20 Gyr, and extinction between 0.00 and 1.00.We list both the mass currently in stars ($M_{\rm stellar}$), and the total baryonic mass ($M_{\rm total}$, which includes the mass returned to the IGM by evolved stars) for each star formation history.

| Model | Reduced $\chi^2_{\rm min}$ | Age (Myr) | $E(B-V)$ | $M_{\rm tot}$ ($10^{10}$ M$_\odot$) | $M_{\rm stellar}$ ($10^{10}$ M$_\odot$) | Current SFR (M$_\odot$ yr$^{-1}$) | $b$ ($10^{-10}$ yr$^{-1}$) |
|---|---|---|---|---|---|---|---|
| burst (SSP) | 1.54 | 114 | 0.00 | 1.32 | 1.09 | 0.00[a] | 0.00 |
| $\tau = 10$ Myr | 1.50 | 128 | 0.00 | 1.35 | 1.13 | 0.02[a] | 0.02 |
| $\tau = 30$ Myr | 1.30 | 161 | 0.01 | 1.42 | 1.17 | 2.23[a] | 1.91 |
| $\tau = 70$ Myr | 0.99 | 255 | 0.00 | 1.59 | 1.29 | 6.12 | 4.74 |
| $\tau = 100$ Myr | 0.87 | 321 | 0.00 | 1.83 | 1.47 | 7.70 | 5.24 |
| $\tau = 300$ Myr | 0.77 | 641 | 0.00 | 2.77 | 2.18 | 12.4 | 5.69 |
| $\tau = 500$ Myr | 0.78 | 905[b] | 0.00 | 3.57 | 2.76 | 14.0 | 5.07 |
| $\tau = 1000$ Myr | 0.81 | 1280[b] | 0.00 | 4.54 | 3.48 | 17.5 | 5.03 |
| continuous | 0.93 | 2600[b] | 0.02 | 4.34 | 3.35 | 16.7 | 4.99 |

[a]Ruled out because SFR below lower limit set by Ly$\alpha$ emission. [b]Ruled out as age is close to or exceeds 1 Gyr, age of Universe at $z \approx 6$.

**Table 5.** Favoured model parameters of various SED fits for SBM03#3, metallicity = $Z_\odot$. We varied age between 0 and 20 Gyr, and extinction between 0.00 and 1.00. We list both the mass currently in stars ($M_{\rm stellar}$), and the total baryonic mass ($M_{\rm total}$, which includes the mass returned to the IGM by evolved stars) for each star formation history.

| Model | Reduced $\chi^2_{\rm min}$ | Age (Myr) | $E(B-V)$ | $M_{\rm tot}$ ($10^{10}$ M$_\odot$) | $M_{\rm stellar}$ ($10^{10}$ M$_\odot$) | Current SFR (M$_\odot$ yr$^{-1}$) | $b$ ($10^{-10}$ yr$^{-1}$) |
|---|---|---|---|---|---|---|---|
| burst | 3.66 | 47.5 | 0.00 | 1.12 | 0.97 | 0.00[a] | 0.00 |
| $\tau = 10$ Myr | 3.65 | 64.1 | 0.00 | 1.17 | 1.02 | 1.93[a] | 1.89 |
| $\tau = 30$ Myr | 3.21 | 114 | 0.00 | 1.53 | 1.29 | 11.7 | 9.07 |
| $\tau = 70$ Myr | 2.75 | 203 | 0.00 | 2.22 | 1.84 | 18.6 | 10.1 |
| $\tau = 100$ Myr | 2.55 | 255 | 0.00 | 2.54 | 2.08 | 21.5 | 10.3 |
| $\tau = 300$ Myr | 2.06 | 453 | 0.00 | 3.54 | 2.85 | 33.4 | 11.7 |
| $\tau = 500$ Myr | 1.96 | 641 | 0.00 | 4.78 | 3.77 | 36.8 | 9.76 |
| $\tau = 1000$ Myr | 1.88 | 905[b] | 0.00 | 6.81 | 5.37 | 46.3 | 8.62 |
| continuous | 1.82 | 1800[b] | 0.00 | 5.20 | 4.02 | 28.9 | 7.19 |

[a]Ruled out because SFR below lower limit set by Ly$\alpha$ emission. [b]Ruled out as age is close to or exceeds 1 Gyr, age of Universe at $z \approx 6$.

rate is declining, or that the current burst was preceded by a more significant episode of star formation.

Hence we next considered a range of more realistic models including an exponentially decaying star formation rate (SFR), such that the current $\mathrm{SFR}_t = \mathrm{SFR}_0\, \mathrm{e}^{-t/\tau}$, where $\mathrm{SFR}_0$ is the star formation rate at the onset of the burst and $\tau$ is the decay time in Myr. Such models are intermediate between SSP ($\tau \to 0$) and continuous star formation ($\tau \to \infty$) models. We considered several values of $\tau$ ranging between 10 Myr to 1 Gyr. As before, those models with ages older than the Universe at $z \approx 6$ were rejected. Also, models with $\tau = 10$ Myr were disregarded as they yielded current SFRs below the lower limit set by the Ly$\alpha$ emission (Section 3.6). The favoured models have an age of $\approx$600 Myr, with decay time-scales of $\tau =$ 300 Myr for SBM03#1, and $\tau = 500$ Myr for SBM03#3.

Finally, we consider a model in which the galaxies are composed of two distinct stellar components: an ongoing starburst at the time of observation and an older population which formed in an instantaneous burst some time previously (Fig. 9). We considered starbursts

**Table 6.** Favoured model parameters of various SED fits for SBM03#3, metallicity = $0.2\,Z_{\odot}$. We varied age between 0 and 20 Gyr, and extinction between 0.00 and 1.00. We list both the mass currently in stars ($M_{\rm stellar}$), and the total baryonic mass ($M_{\rm total}$, which includes the mass returned to the IGM by evolved stars) for each star formation history.

| Model | Reduced $\chi^2_{\rm min}$ | Age (Myr) | $E(B-V)$ | $M_{\rm tot}$ ($10^{10}\,M_{\odot}$) | $M_{\rm stellar}$ ($10^{10}\,M_{\odot}$) | Current SFR ($M_{\odot}\,{\rm yr}^{-1}$) | $b$ ($10^{-10}\,{\rm yr}^{-1}$) |
|---|---|---|---|---|---|---|---|
| burst | 2.15 | 71.9 | 0.00 | 1.38 | 1.17 | 0.00[a] | 0.00 |
| $\tau = 10$ Myr | 2.12 | 80.6 | 0.00 | 1.30 | 1.12 | 0.41[a] | 0.37 |
| $\tau = 30$ Myr | 1.92 | 128 | 0.00 | 1.51 | 1.26 | 7.21 | 5.72 |
| $\tau = 70$ Myr | 1.73 | 203 | 0.00 | 1.81 | 1.50 | 15.2 | 10.1 |
| $\tau = 100$ Myr | 1.67 | 255 | 0.00 | 2.07 | 1.69 | 17.5 | 10.4 |
| $\tau = 300$ Myr | 1.50 | 453 | 0.00 | 2.96 | 2.37 | 27.9 | 11.8 |
| $\tau = 500$ Myr | 1.46 | 571 | 0.00 | 3.65 | 2.90 | 34.2 | 11.8 |
| $\tau = 1000$ Myr | 1.41 | 806[b] | 0.00 | 5.37 | 4.22 | 43.3 | 10.3 |
| continuous | 1.36 | 1400[b] | 0.00 | 4.34 | 3.44 | 25.1 | 7.30 |

[a]Ruled out because SFR below lower limit set by Ly$\alpha$ emission. [b]Ruled out as age is close to or exceeds 1 Gyr, age of Universe at $z \approx 6$.

**Table 7.** Two-population composite models for SBM03#1, assuming an ongoing burst of constant star formation rate, commencing 3–100 Myr ago, within an older galaxy. The best-fitting galaxy age and mass fraction of the starburst for each model are tabulated (for solar metallicity, $Z_{\odot}$).

| Burst duration (Myr) | Reduced $\chi^2$ | Fraction of mass | Current SFR ($M_{\odot}\,{\rm yr}^{-1}$) | Age (Myr) | Stellar mass ($10^{10}\,M_{\odot}$) |
|---|---|---|---|---|---|
| 3 | 0.71 | 0.5 per cent | 60.0 | 400 | 3.6 |
| 10 | 0.68 | 0.7 per cent | 25.3 | 450 | 3.6 |
| 30 | 0.72 | 1.7 per cent | 19.0 | 450 | 3.3 |
| 100 | 0.79 | 5.2 per cent | 68.3 | 450 | 3.1 |

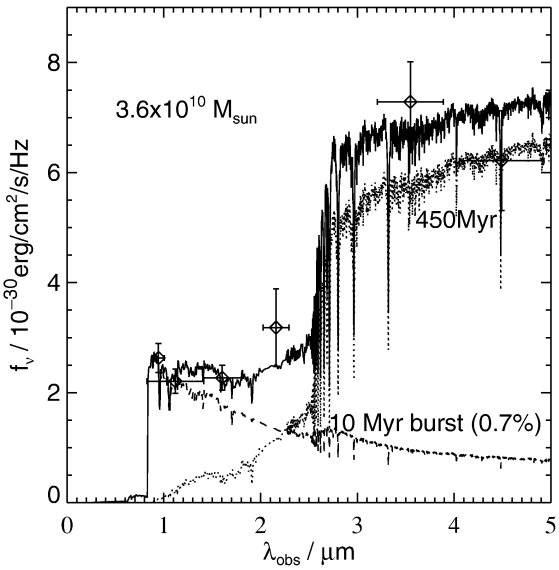


**Figure 9.** The best-fitting two-component stellar population model (Salpeter IMF) for SBM03#1: a dominant 450-Myr population of mass $3.6 \times 10^{10}\,M_{\odot}$, with some ongoing star formation activity (a burst for the last 10 Myr involving 0.7 per cent of the stellar mass). Using a Chabrier IMF produces an identical best-fitting age, with a similar mass fraction in the burst (0.6 per cent), but a 30 per cent lower total stellar mass ($2.5 \times 10^{10}\,M_{\odot}$).

with a constant SFR which started 3, 10, 30 and 100 Myr prior to the epoch of observation. We varied the ratio of total stellar masses in these two populations, and found the best-fitting ages for the old component to be 400–500 Myr. From the best-fitting models (Table 7), the fraction of total stellar mass being formed in the starburst is 0.5–5 per cent for starbursts of 3–100 Myr duration.

In summary, our SED fitting shows that the broad-band colours can be fit with a variety of stellar ages/star formation histories. The lower limit on the age is >100 Myr (from an SSP model) with the oldest allowed models comparable to the age of the Universe at $z \approx 6$. Our best fits to the broad-band photometry come from exponentially decaying star formation histories, or a two-component model where only 0.5–5 per cent of the stellar mass is forming in an ongoing starburst. These best-fitting models have mean stellar ages of 260–640 Myr, which would require formation redshifts of $z_{\rm f} \approx 7.5$–13.5.

It has been speculated that certain treatments of the thermally pulsing asymptotic giant branch (TP-AGB) may lead to different age estimates from broad-band colours. Maraston (2005) suggests the $z \sim 2$–3 population of 'iEROs' identified by Yan et al. (2004) in *HST*+*Spitzer* images can be fit by younger ages than indicated by the Bruzual & Charlot (2003) models. Potentially the TP-AGB has a significant impact on the rest frame $V-K$ colours measured in the ACS/IRAC images at $z \approx 2$–3. However, our $i'$-drops are at higher redshifts, and the TP-AGB has little effect at $\lambda < 0.7\,\mu$m (see fig. 14 of Maraston 2005), the wavelength range which we are probing with our *HST*+*Spitzer* detections.

### 3.3 Stellar masses at $z \approx 6$

The SED fitting procedure described above leaves the normalization of the Bruzual & Charlot model as a free parameter (along with the age for a particular input model). Our code outputs this normalization and, by using the luminosity distance to the $i'$-drop galaxies, we can calculate the corresponding best-fitting stellar mass for each star formation history. Tables 3, 4, 5 and 6 give the best-fitting masses returned by the SED fitting. We list both the mass

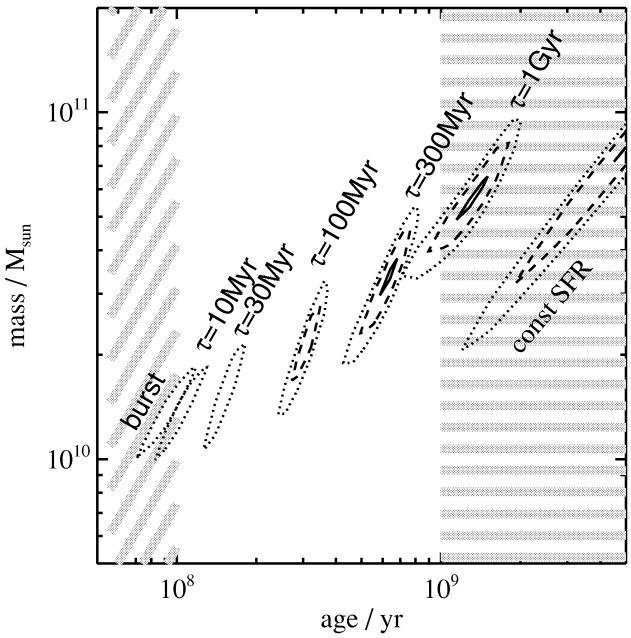


**Figure 10.** The allowed range of masses for several exponentially decaying SFR models for SBM03#1, with decay times ranging from $\tau = 10$–1000 Myr, as well as an instantaneous burst model and a constant SFR model. Those with stellar ages $>1$ Gyr (right shaded region) are ruled out (the Universe is younger than this at $z \approx 6$). The models with ages $< 10^8$ yr are also excluded as they fail to produce the observed current SFR inferred from Ly$\alpha$ emission (left shaded region). Contours are 68 per cent confidence (solid line), 95 per cent confidence (dashed line) and 99 per cent confidence (dotted line) for reduced $\chi^2$ of $\approx$1, 2, 3.

currently in stars ($M_{\rm stellar}$) and the total baryonic mass ($M_{\rm total}$, which includes the mass returned to the IGM by evolved stars) for each star formation history. To assess the errors on the stellar mass estimates, we took the best-fitting mass, $M_{\rm stellar}$, and recalculated the reduced $\chi^2$ for the same age, metallicity and star formation history, but using total masses in the range $0.1 - 3\,M_{\rm stellar}$ (shown in Fig. 10). In all our models, the stellar masses of SBM03#1 and #3 were $>10^{10}\,{\rm M}_\odot$ at 95 per cent confidence ($2\sigma$). The lowest masses were returned by the SSP model, and by the exponentially decaying models with short decay times ($\tau \sim 10$ Myr): in fact, these models are unable to provide sufficient ongoing star formation to explain the lower limit set on the star formation rate by the Ly$\alpha$ emission (see Section 3.6). Our preferred models ($\tau = 70$–500 Myr and the two-component stellar population) have stellar masses of $\approx$2–4 $\times\ 10^{10}\,{\rm M}_\odot$ for a Salpeter IMF (we consider the impact of adopting a Chabrier IMF in Section 3.5).

We measure stellar masses from the best-fitting SEDs of $M > 2 \times 10^{10}\,{\rm M}_\odot$ at $z \approx 6$. This is surprisingly large, supporting our contention that at least these two objects are well-established galaxies. The stellar mass is equivalent to 20 per cent of that for a $L^*$ galaxy today, using $L_r^* = -21.21$ from the SDSS analysis of Blanton et al. (2003) and taking $M/L_V \approx 5\,{\rm M}_\odot/{\rm L}_\odot$ (appropriate for a $\approx$10 Gyr old population from B&C models using a Salpeter IMF) to obtain $M^* = 1.2 \times 10^{11}\,{\rm M}_\odot$, comparable to the estimate of $M^* = 1.4 \times 10^{11}\,{\rm M}_\odot$ from Cole et al. (2001) for our adopted Salpeter IMF.

### 3.4 Stellar mass density and the Kormendy relation

A key question, given the increased information content on our two $z \approx 6$ sources, is the likely descendant population and connection with systems seen at lower redshift. In this respect, we now consider the high surface brightness and small angular extent of the $i'$-drop galaxies.

To facilitate this discussion, we examine the properties of the $z \approx 6$ galaxies with reference to the $z \sim 0$ Kormendy relation between galaxy surface brightness and half-light radius (Kormendy 1977). Both SBM03#1 and #3 have half-light radii (effective radii) of $r_{\rm hl} \approx 0.08$ arcsec (Bunker et al. 2003, 2004), and IRAC total magnitudes of $AB \approx 24$ at 3.6 μm (corresponding to the rest-frame $V$-band). The average surface brightness *within* the effective radius, $\langle I \rangle_{\rm hl}$, is related to the average surface brightness *at* $r_{\rm hl}$, $I_{\rm hl}$, by $\langle I_{\rm hl} \rangle = 3.6 \times \langle I \rangle_{\rm hl}$ for a de Vaucouleurs profile (Ciotti & Bertin 1999). Hence our surface brightness at $r_{\rm hl}$ is $\mu_e = 21.6\,{\rm mag\,arcsec^{-2}}$.

Cosmological surface brightness dimming of $(1+z)^4$ would have dimmed *real* surface brightnesses by +8.3 mag, and passive evolution from an age of $\approx$200 Myr at $z = 5.8$ to 12.8 Gyr at $z = 0$ would produce a luminosity dimming of a factor of $\times$ 30 in $V$ (+3.7 mag, using the B&C models). Hence, we might expect SBM03#1 and #3 to have surface brightnesses *today* of $\mu_e = 21.6 - 8.3 + 3.7 = 17.0\,{\rm mag\,arcsec^{-2}}$ for their half-light radii of $r_{\rm hl} = 0.4$ kpc. In fact, the passively evolved surface brightnesses sit comfortably on the present-day Kormendy relation (e.g. that of Ziegler et al. 1999 for cluster ellipticals), extrapolated to smaller scalelengths. Hence it seems that the inferred properties of these $z \approx 6$ galaxies are compatible with galaxy scaling relations at $z = 0$, subject to dimming through stellar evolution. Although our analysis has focused on only two of the most luminous systems, chosen by virtue of their luminosity, the possible implications are profound. What do these $i'$-drop galaxies at $z \approx 6$ evolve into? Given that these objects are barely resolved in the *HST* /ACS data with $r_{\rm hl} < 0.5$ kpc, they are unlikely to passively evolve into the ellipticals we see in the present-day Universe – these are typically larger. Merging would be required to explain the size evolution, although we note that the stellar masses and spatial scales of our $z \approx 6$ galaxies are similar to those of some spiral bulges today: a stellar age of $\approx$12 Gyr (Wyse, Gilmore & Franz 1997) today would imply a formation epoch of $z > 5$.

### 3.5 Effects of metallicity, dust and IMF on SED fitting

When conducting the SED fitting, two metallicities were considered: solar ($Z_\odot$) and a sub-solar model ($0.2\,Z_\odot$). The ages and masses of the best-fitting models were similar for both metallicities, although the sub-solar model returned slightly better fits to the data, with smaller reduced $\chi^2_{\rm min}$ values.

We also considered whether the red optical–infrared colours (spanning the rest-frame UV to optical) could be attributable to dust reddening instead of, or as well as, an underlying old stellar population. To further examine this, we adopt the reddening model of Calzetti (1997),[7] appropriate to starburst galaxies. We constructed a grid of models for both the SSP (instantaneous burst) and constant SFR scenarios, using the Bruzual & Charlot templates over the full range of 221 age steps. For each age, we varied reddening

[7] The Calzetti reddening is an empirical law is given in terms of the colour excess $E(B-V) = 0.44\,E_{\rm gas}\,(B-V)$ with the wavelength dependence of the reddening expressed as:
$k(\lambda) = 2.656(-2.156 + 1.509\lambda^{-1} - 0.198\lambda^{-2} + 0.011\lambda^{-3}) + 4.88$
for $0.12\ \mu{\rm m} \leqslant \lambda \leqslant 0.63\ \mu{\rm m}$, and
$k(\lambda) = [(1.86 - 0.48\lambda^{-1})/(\lambda - 0.1)]/\lambda + 1.73$
for $0.63\ \mu{\rm m} \leqslant \lambda \leqslant 1.0\ \mu{\rm m}$, and the flux attenuation is given by:
$F_{\rm obs}(\lambda) = F_0(\lambda)\,10^{-0.4E(B-V)k(\lambda)}$.

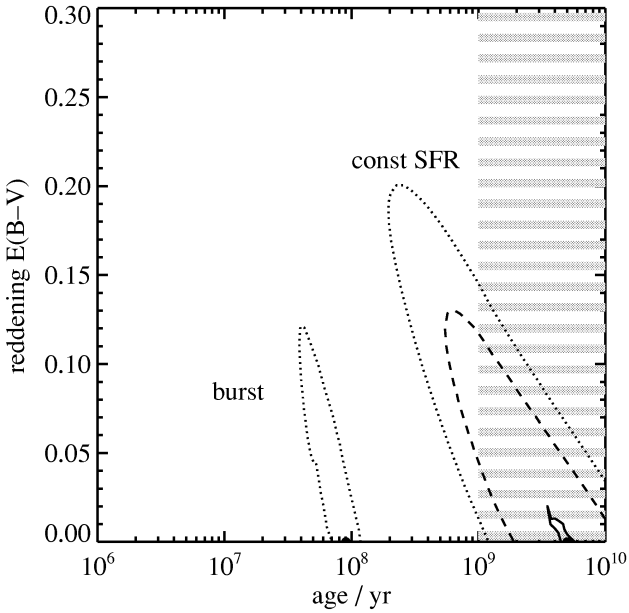


**Figure 11.** SBM03#1: A plot showing the reddening $E(B-V)$ values for the two limiting scenarios of an instantaneous burst model and a constant SFR model, for the case metallicity $= Z_{\odot}$. Contours are 68 per cent confidence (solid line), 95 per cent confidence (dashed line) and 99 per cent confidence (dotted line) for reduced $\chi^2$ of $\approx$1, 2, 3.

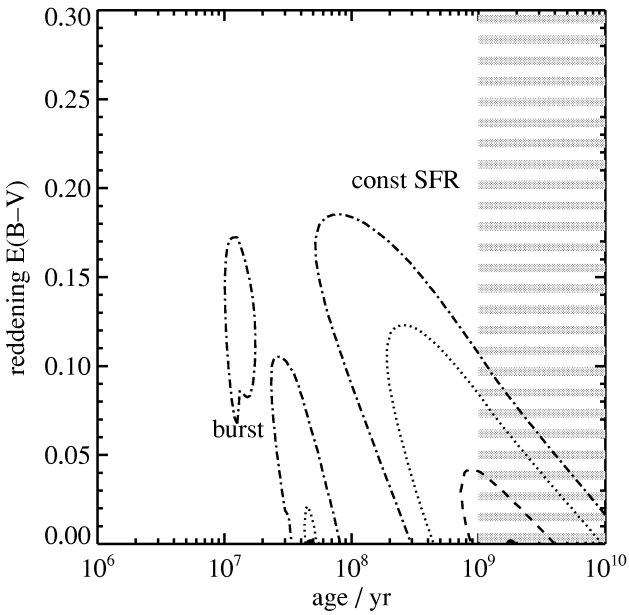


**Figure 12.** As Fig. 11, but for SBM03#3. Contours are for reduced $\chi^2$ of $\approx$1, 2, 3 and 4, corresponding to 68 per cent confidence (solid line), 95 per cent confidence (dashed line), 99 per cent confidence (dotted line), and $4\sigma$ confidence (dot-dash line).

in the range $E(B-V) = 0.00 - 1.00$ mag, in steps of 0.01 mag, computing the reduced $\chi^2$ at each step. We find little evidence for substantial dust reddening in the detected starlight out to $\approx$5 μm: the formal best fits for both SBM03#1 and #3 are 'no reddening' (Figs 11 and 12). This is consistent with the flat spectral slopes in $f_\nu$ between the ACS $z'$-band and the NICMOS $J$- and $H$-bands reported by Stanway et al. (2005) for many of the $i'$-drops in the *Hubble* Ultra Deep Field, including SBM03#1. The brightening in $f_\nu$ flux between the near-infrared (0.8–2.2 μm) and the IRAC bands at 3–5 μm is best explained by a spectral break rather than by the smoother continuum gradient produced by dust reddening, and this is reflected in the best-fitting stellar populations.

Finally, we tested the effects on the derived stellar masses of the assumed initial mass function. For the galaxy SBM03#1 (where the multi-waveband data was best, as it included NICMOS imaging in the near-infrared), we re-ran the 'two-population' model fits (Section 3.2) with a Chabrier (2003) IMF, instead of a Salpeter (1955) power-law IMF. We used the same ongoing 10 Myr constant star formation rate burst, and fit for the age of an underlying older stellar population and the relative stellar masses of the burst and the old stars. Both IMFs produced comparably good fits (near-identical $\chi^2$ values), the same 450 Myr ages, and near-identical burst fractions (0.6 per cent and 0.7 per cent by mass for the Chabrier and Salpeter IMFs). The main difference came in the best-fitting total stellar mass: the Chabrier model produced a mass $\approx$30 per cent less than the Salpeter IMF ($2.5 \times 10^{10}\,M_{\odot}$ compared with $3.6 \times 10^{10}\,M_{\odot}$ for SBM03#1). This effect is mainly a mass re-scaling independent of star formation history, as the discrepancy primarily arises from the different mass fraction in long-lived low-mass stars.

### 3.6 Star formation rates

We can usefully compare the ongoing star formation rate, the stellar mass and implied age, to deduce whether our two selected $z \approx 6$ galaxies are being seen during a fairly quiet or an active period in their history.

First, let us consider the ongoing SFR. Star formation will dominate the rest-frame UV light (probed by the *HST*/ACS images) in the absence of dust obscuration or a significant AGN contribution. In our first analyses of $i'$-drop galaxies in the GOODS ACS images (Stanway et al. 2003, 2004a) and the Ultra Deep Field (Bunker et al. 2004), we used the conversion from rest-frame UV flux density to SFR, given by Madau, Pozzetti & Dickinson (1998), appropriate for continuous star formation. Based on the $z'$-band magnitudes we inferred unobscured SFRs of 19.5 and 33.8 $M_{\odot}\,yr^{-1}$ for SBM03#1 & #3, after accounting for Lyman forest blanketing of $D_A \approx 0.95$ shortwards of Ly$\alpha$.

The fits of the Bruzual & Charlot stellar synthesis models to the broad-band photometry provide estimates of the current SFR for a range of histories (Tables 3–7). However, a firm lower limit arises from our Keck/DEIMOS spectroscopy (Bunker et al. 2003; Stanway et al. 2004a), which revealed Ly$\alpha$ emission. If this line emission is powered by ionizing photons from OB stars, then there must be star formation activity in these galaxies within the past 10 Myr (the lifetime of these stars, which dominate the Lyman continuum flux).

We have argued previously that the absence of X-ray emission and high-ionization lines such as N *V* 1240 Å, coupled with the narrow velocity width of the Ly$\alpha$ emission, renders an AGN interpretation unlikely. Our spectroscopy of SBM03#1 & #3 indicates line fluxes of $2 \times 10^{-17}$ erg s$^{-1}$ cm$^{-2}$ for both sources, with rest-frame equivalent widths of $W_{\rm rest} = 30$, 20 Å. Assuming case B recombination and the same Salpeter IMF as in the Bruzual & Charlot models, the star formation rates from Ly$\alpha$ are $\approx 6\,M_{\odot}\,yr^{-1}$. This may be treated as a firm *lower limit* on the current SFR, as the resonantly scattered Ly$\alpha$ line is invariably quenched by dust to well below its case B line strength.

Our spectroscopic lower limit of an SFR $> 6\,M_{\odot}\,yr^{-1}$ rules out the simple SSP model and those declining star formation rate

models with the shortest decay times ($\tau = 10$–$30$ Myr, see Fig. 10). Our favoured models are an exponentially decaying SFR with decay time $\tau \approx 300$–$500$ Myr, and two-component models with 1–2 per cent of the stellar mass created in an ongoing starburst which began 10–100 Myr prior to the epoch of observation. These all indicate similar SFRs to our original estimates of $\approx 20$–$30\,M_\odot\,yr^{-1}$ from the $z'$-band flux.

Returning to the ratio of the current SFR to the stellar mass already formed, it is helpful to consider the '$b$-parameter' (e.g. Brinchmann et al. 2004) – a measure of the fraction of the total stellar mass currently being born as stars, defined as $b = \mathrm{SFR}/M_{\mathrm{stellar}}$. We measure $b \approx 5$ and $10 \times 10^{-10}\,yr^{-1}$ for SBM03#1 and #3, comparable with the values inferred by Egami et al. (2005) from the *Spitzer* image of a lensed galaxy with a photometric redshift of $z \approx 7$ (Kneib et al. 2004), and an indication of vigorous current star formation which supports the conclusion of this paper. However, the past-average SFR must actually be *greater* than the current SFR in order to build our $\approx 2 \times 10^{10}\,M_\odot$ galaxies, given the short time available prior to $z \approx 6$ (1 Gyr). This is why decaying SFR models appear to give the best fits to the SEDs. Juneau et al. (2005) define a characteristic growth time-scale (in a study of $z \sim 1$ galaxies), with $t_{\mathrm{SFR}} = M_{\mathrm{stellar}}/\mathrm{SFR} = 1/b$. The ratio of this to the Hubble time at that epoch, $t_{\mathrm{H}}(z)$, can be interpreted as galaxies in a declining or quiescent star formation mode if $t_{\mathrm{SFR}} > t_{\mathrm{H}}$. This is the case for both SBM03#1 and #3 for the best-fitting models. Indeed, to form the $2$–$4 \times 10^{10}\,M_\odot$ of stars requires an average star formation rate of $50$–$100\,M_\odot\,yr^{-1}$ over the redshift range $z_{\mathrm{f}} = 7.5$–$13.5$ favoured for the formation of the old stellar component (Section 3.2). Hence, $\langle \mathrm{SFR}_{\,z=7.5-13.5} \rangle / \langle \mathrm{SFR}_{\,z=6} \rangle \approx 2$–$5$; the past-average star formation rates of SBM03#1 and #3 are factors of 2–5 greater than their current rates at the epoch of observation ($z \approx 5.8$).

Although our chosen galaxies are the brightest confirmed $i'$-drops in the GOODS-South field and possibly unrepresentative, the present work does imply that in these galaxies at least there was a yet earlier vigorous phase of activity, possibly at $z > 10$, which may have played a key role in reionizing the Universe. This may be consistent with the measurement of temperature-polarization correlation of the cosmic microwave background from the *Wilkinson MAP* satellite by Kogut et al. (2003).

## 4 CONCLUSIONS

Our group previously identified and spectroscopically confirmed $z \approx 6$ galaxies through *HST*/ACS $i'$-drop imaging, as well as through Keck/DEIMOS and Gemini/GMOS spectroscopy. This paper presents the first infrared detections of this population using *Spitzer*/IRAC. We have significant ($\approx 10\sigma$, $AB \approx 24$ mag) detections at 3.6 μm of the Stanway et al. (2003) galaxies #1 and #3 (at $z_{\mathrm{spec}} = 5.83, 5.78$), and a more marginal detection of the $z_{\mathrm{spec}} = 5.79$ galaxy GLARE#3001 (Stanway et al. 2004b). We also detect SBM03#1 at 4.5 μm (SBM03#3 is outside the field of view of this 4.5 μm filter).

We infer from Ly$\alpha$ emission in our discovery spectra that there is ongoing star formation of $>6\,M_\odot\,yr^{-1}$ (as would be expected in these rest-UV-selected objects). However, the preceding star formation history has not been explored until now. In the two best-detected galaxies, we have evidence of a significant Balmer/4000-Å break, indicative of a prominent older stellar population which probably dominates the stellar mass. Exploring a range of population synthesis models indicates that the average stellar age is $>100$ Myr; our best-fitting models suggest preferred ages of $250 - 650$ Myr for an exponentially declining star formation rate (of decay time $\tau \approx$ 70–500 Myr) or a two-component model (with an ongoing starburst responsible for 0.5–5 per cent of the total stellar mass). This implies formation epochs of $z_{\mathrm{f}} \approx 7.5$–$13.5$ for the galaxies SBM03#1 and #3.

In all our models, the best-fitting stellar masses are $>10^{10}\,M_\odot$, with 95 per cent confidence masses of $1.3$–$3.8 \times 10^{10}\,M_\odot$. This indicates that at least some galaxies with stellar masses >20 per cent of the mass of $L^*$ galaxies today were already assembled within the first Gyr of the Universe. For these objects, the past average star formation rate is comparable to, or greater than, the current SFR, implying that there may have been even more vigorous episodes of star formation at higher redshifts. These may have played a key role in reionizing the Universe, consistent with the earlier studies of Bunker et al. (2004) and Egami et al. (2005).

## ACKNOWLEDGMENTS

We thank Karl Glazebrook, Rychard Bouwens, Richard McMahon, Rodger Thompson and the anonymous referee for very useful comments. This work is based [in part] on observations made with the *Spitzer Space Telescope*, which is operated by the Jet Propulsion Laboratory, California Institute of Technology under NASA contract 1407. Observations have been carried out using the Very Large Telescope at the ESO Paranal Observatory under Program ID: LP168.A-0485. This paper is based in part on observations made with the NASA/ESA *Hubble Space Telescope*, obtained from the Data Archive at the Space Telescope Science Institute, which is operated by the Association of Universities for Research in Astronomy, Inc., under NASA contract NAS 5-26555. These observations are associated with proposals #9425 & 9583 (the GOODS public imaging survey). We are grateful to the GOODS team for making their reduced images public – a very useful resource. LPE acknowledges a Particle Physics and Astronomy Research Council (PPARC) studentship supporting this study.

## REFERENCES

Barmby P. et al., 2004, ApJS, 154, 97
Becker R. H. et al., 2001, AJ, 122, 2850
Beckwith S., Somerville R., Stiavelli M., 2003, STScI Newsletter Vol., 20, issue 04 (http://sco.stsci.edu/newsletter/PDF/2003/fall_03.pdf)
Blanton M. R. et al., 2003, ApJ, 592, 819
Bouwens R. J. et al., 2004a, ApJL, 606, 25
Bouwens R. J. et al., 2004b, ApJL, 616, 79
Bouwens R. J., Illingworth G. D., Thompson R. I., Franx M., 2005, ApJL, 624, 5
Brinchmann J., Charlot S., White S. D. M., Tremonti C., Kauffmann G., Heckman T., Brinkmann J., 2004, MNRAS, 351, 1151
Bruzual G. A., 1983, ApJ, 273, 105
Bruzual G. A., Charlot S., 2003, MNRAS, 344, 1000
Bunker A. J., Stanway E. R., Ellis R. S., McMahon R. G., McCarthy P. J., 2003, MNRAS, 342, L47
Bunker A. J., Stanway E. R., Ellis R. S., McMahon R. G., 2004, MNRAS, 355, 374
Calzetti D., 1997, AJ, 113, 162
Chabrier G., 2003, PASP, 115, 763
Ciotti L., Bertin G., 1999, A&A, 352, 447
Cole S. et al., 2001, MNRAS, 326, 255
Dickinson M., Giavalisco M., 2003, in Bender R., Renzini A., Proc. ESO Workshop, The Mass of Galaxies at Low and High Redshift. Springer, Berlin, p. 3224
Dickinson M. E. et al., 2004, ApJL, 600, 99
Egami E. et al., 2005, ApJL, 618, 5
Fazio G. G. et al., 2004, ApJS, 154, 10

Ford H. C. et al., 2003, SPIE, 4854, 81
Giacconi R. et al., 2002, ApJS, 139, 369
Giavalisco M., 2003, AAS, 202, 1703
Giavalisco M. et al., 2004, ApJL, 600, 103
Juneau S. et al., 2005, ApJL, 619, 135
Kauffmann G. et al., 2003, MNRAS, 341, 33
Kneib J.-P., Ellis R. S., Santos M. R., Richard J., 2004, ApJ, 607, 697
Kodaira K. et al., 2003, PASJ, 55, L17
Kogut A. et al., 2003, ApJS, 148, 161
Kormendy J., 1977, ApJ, 217, 406
Lacy M. et al., 2005, submitted to ApJS
Le Borgne D. et al., 2005, ApJ, submitted (astro-ph/0503401)
Liu M. C., Graham J. R., Charlot S., 2002, ApJ, 564, L216
Madau P., Pozzetti L., Dickinson M., 1998, ApJ, 498, 106
Malhotra S. et al., 2005, ApJ, 626, 666
Maraston C., 2005, MNRAS, 362, 799
Oke J. B., Gunn J. E., 1983, ApJ, 266, 713
Peng C. Y., Ho L. C., Impey C. D., Rix H.-W., 2002, AJ, 124, 266
Reach W. T., Surace J., Glaccum W.J., Carey S.J., Lacy M., Brandenburg H., Lowrance P., Im M., 2004, in Surace J.A., Lowrance P., eds, Infrared Array Camera Data Handbook version 1.0. Spitzer Science Center, California Institute of Technology, Pasadena CA
Rhoads J. E. et al., 2004, ApJ, 611, 59
Salpeter E. E., 1955, ApJ, 121, 161
Shapley A. E., Steidel C. C., Erb D. K., Reddy N. A., Adelberger K. L., Pettini M., Barmby P., Huang J., 2005, ApJ, 626, 698
Spergel D. N. et al., 2003, ApJS, 148, 175
Stanway E. R., Bunker A. J., McMahon R. G., 2003, MNRAS, 342, 439
Stanway E. R., Bunker A. J., McMahon R. G., Ellis R. S., Treu T., McCarthy P.J., 2004a, ApJ, 607, 704
Stanway E. R. et al., 2004b, ApJ, 604, L13
Stanway E. R., McMahon R. G., Bunker A. J., 2005, MNRAS, 359, 1184
Steidel C. C., Pettini M., Hamilton D., 1995, AJ, 110, 2519
Steidel C. C., Giavalisco M., Pettini M., Dickinson M. E., Adelberger K. L., 1996, ApJ, 462, L17
Steidel C. C., Adelberger K. L., Giavalisco M., Dickinson M. E., Pettini M., 1999, ApJ, 519, 1
Thompson R. I. et al., 2005, AJ, 130, 1
Vassiliadis E., Wood P. R., 1993, ApJ, 413, 641
Wyse R. F. G., Gilmore G., Franz M., 1997, ARA&A, 35, 637
Yan H., Windhorst R. A., 2004, ApJ, 612, L93
Yan H. et al., 2004, ApJ, 616, 63
Ziegler B. L., Saglia R. P., Bender R., Belloni P., Greggio L., Seitz S., 1999, A&A, 346, 13

This paper has been typeset from a TEX/LATEX file prepared by the author.